IEEE Access
Multidisciplinary | Rapid Review | Open Access Journal

Received March 21, 2020, accepted April 5, 2020, date of publication April 13, 2020, date of current version April 29, 2020.

Digital Object Identifier 10.1109/ACCESS.2020.2987621

Centralized MPPT Controller System of PV Modules by a Wireless Sensor Network

ARANZAZU D. MARTIN[1], J. M. CANO[1], J. MEDINA-GARCÍA[2], J. A. GÓMEZ-GALÁN[2], AND JESUS R. VAZQUEZ[1]

[1]Department of Electrical Engineering, University of Huelva, 21007 Huelva, Spain
[2]Department of Electronic Engineering, Computers, and Automation, University of Huelva, 21007 Huelva, Spain

Corresponding author: Aranzazu D. Martin (aranzazu.delgado@die.uhu.es)

ABSTRACT An efficient monitoring and control system for solar photovoltaic modules, which combines the use of a non-linear MPPT backstepping controller with a custom wireless sensor network (WSN) has been developed. The infrastructure consists of a wireless smart photovoltaic system (WSPS) and a wireless centralized control system (WCC). The data of sensing, coordination and control is handled by using a WSN based on IEEE 802.15.4 technology in beacon enable mode and with guaranteed time slot. This assures the data transmission and a synchronous acquisition, which are critical elements in a wireless photovoltaic monitoring system. All measured data is gathered by an autonomous, compact and low-cost sensor node installed in each PV module, and it is transferred to the coordinator node. The power consumption of the sensor node represents only 0.25% of the power delivered by the photovoltaic module. A backstepping controller to track the Maximum Power Point (MPP) by means of a buck-boost converter derives the reference parameters to return to each PV module accordingly. The wireless solution uses low latency techniques to achieve a real-time monitoring and a stable performance of the controller. The centralized control identifies all the network nodes and significantly simplifies the maintenance operations. Experimental validation shows the robustness against interference and security in the wireless data transmission and confirms the feasibility of the proposed wireless sensor system in tracking the maximum power transfer under different weather conditions, achieving an efficiency over the 99% in the MPPT.

INDEX TERMS Backstepping control, photovoltaic monitoring systems, IEEE 802.15.4 communication, wireless sensor network

I. INTRODUCTION

In recent years, a new generation of sensors has emerged, which are independent of a specific electronic system and that incorporate in the same device the transducer (of the variable or variables that are of interest to measure), the power supply, and a communication module equipped with a certain intelligence, capable of organizing itself, of having a certain computing capacity, and of executing protocol and encryption algorithms, in addition to wirelessly interconnecting with other nodes similar to it. The idea is to create an environment in which the basic information from any of the connected autonomous elements can be shared efficiently and in real-time [1].

The associate editor coordinating the review of this manuscript and approving it for publication was Kok Lim Alvin Yau.

As a result of this deployment, the so-called wireless sensor networks (WSN) have emerged, which contain a multitude of individual sensors that exchange information with each other and/or with a centralized node, without the need for cables and through a pre-established communication protocol [2]. Each of the nodes of the network is connected to one or more devices. The nodes that make measurements are commonly called sensor nodes. Those who are responsible for retransmitting data are called routers. Finally, there is a node responsible for centralizing the information and exchanging it with other networks, called the base station, sink node or gateway. The user can control the network through the base station. Aspects such as data rate, latency, synchronization, robustness against interference, security and quality of service (QoS) are parameters to be considered in the design of the WSN.

In addition to the WSN, the use of renewable energy sources is also widespread in last years. Specifically, the photovoltaic systems and the distributed photovoltaic generation are rapidly developing around the world. As it is widely known that PV systems have relatively low efficiency, optimizing the energy extraction and reliability and reducing the losses is essential. Besides, the selection of the power converter also plays an important role in the overall power losses. In this work, a distributed PV system [3], [4], where each PV module is connected to a different DC/DC converter, is used to reduce the losses due to the mismatching operating conditions [5], since each solar module and power converter have their own control.

As mentioned before, in power plants it is crucial to track the maximum power point (MPP) in real time in order to maximize the generation. For that, it is required to consider that PV systems are nonlinear. A large variety of MPPT algorithms have been developed up to now [6], [7], with different complexities, tracking efficiencies, required sensors, etc. According to the control strategies, the MPPT algorithms are classified as direct, indirect or soft computing control. The direct control technique searches the maximum power point with previous measured parameters or PV characteristic. In this group the well-known P&O is included [8], the incremental conductance method [9] or the ripple correlation control [10], amongst others [6]. The indirect control methods employ empirical data from a database to estimate the MPP by means of mathematical relationships. The MPPTs of this group are the curve fitting [6], the fractional short-circuit current, or the fractional open-circuit voltage, amongst others [7]. The soft computing methods, such as the ones based on fuzzy logic [11], artificial neural networks [12], or particle swarm optimization [13], usually do not require information about the model and obtain more accuracy and robustness. In this work, backstepping control is used [14], [15] in order to make the system robust, stable, and have a computable transient response through Lyapunov functions to guarantee stability.

Other aspects that require taking into consideration are low cost and easy maintenance. For that, the use of wireless signal communication through a WSN can help in PV systems. For instance, if a relocation of the PV modules is required [16], the process reduces costs with the WSN since wires are not necessary. Besides, it is possible to make continuous predictive maintenance, detecting the failures rapidly and solving the malfunctions promptly [17]–[21]. Then, the energy losses are avoided thanks to the monitoring by means of the WSN. The remote monitoring to obtain the sensor data is widely used in other applications and it is also employed in photovoltaics [22], [23]. Apart from achieving the sensor values, the WSN can be used to control the PV system through a controller in order to reach the MPP in real time. Another aspect to take into consideration is the energy consumption of the wireless sensor node, in this case using solar energy harvesters, [24]–[26].

This paper aims to develop a wireless remote monitoring and control system of solar photovoltaic modules. The PV system has a distributed architecture with each PV module being connected to a buck-boost converter, and a non-linear backstepping controller is used to continuously track the local maximum power point with high efficiency. The work demonstrates the development, testing, and utilization of the entire system using embedded IEEE 802.15.4 radio technology. The system is based on a wireless sensor network and includes all the components required to provide real-time monitoring while tracking efficiency. The proper performance of the whole system relies on the operation of the wireless sensor modules attached to each solar cell in order to gather the relevant information and send it to the centralized node. The wireless communication has been designed to operate in beacon-enabled mode and with guaranteed time slot to achieve low data monitoring latency, which ensures the stability of the controller. The wireless sensor nodes meet low power consumption levels since they are supplied from the PV module itself, and other properties such as, small size, low cost, flexibility and, secure and reliable data transmission, all required by WSN designs.

II. WIRELESS PHOTOVOLTAIC DATA TRANSMISSION SYSTEM

It is not easy for the WSN designer to select the most efficient solution in the design of a WSN architecture for a specific application. Wireless technologies, such as 802.11 (Wi-Fi), Bluetooth Low Energy (BLE), Ultra-Wide Band (UWB), ZigBee, IEEE 802.15.4, etc. are available options [27], [28]. In this work, the IEEE 802.15.4 standard has been chosen for communications because in recent years it has become a leading technology for WSN applications with low data rates and high energy efficiency. This standard is a low complexity protocol that further offers low cost, high versatility for the development of different topologies, as well as the transmission of periodic, intermittent and low reaction time data.

A wireless PV monitoring and control system was developed by utilizing wireless sensor networks (WSNs). Although a wired system is potentially more reliable, the wireless transmission provides dynamic mobility, easy relocation, and reduces installation and maintenance costs. The system monitors the efficiency of photovoltaic modules and optimizes the energy production. Through the network some relevant electrical parameters, as well as temperature and irradiance are periodically sampled under practical operation conditions. The measurement data is transferred to the centralized node via the IEEE 802.15.4 standard. After the transmission process, the MPPT control algorithm derives the reference parameters to return to each PV module accordingly.

The system presented in this work includes two different parts, the Wireless Smart Photovoltaic System (WSPS) and the Wireless Centralized Control (WCC). The WSPS consists of the photovoltaic modules, a DC/DC converter

and a network node. The WCC is the control terminal unit (CTU) with the wireless centralized network node (coordinator or host node). The CTU contains the maximum power point tracking (MPPT) and the implemented control, in this case, the backstepping control [14], [15]. The whole system, depicted in Fig. 1, contains different WSPSs connected to achieve higher power.

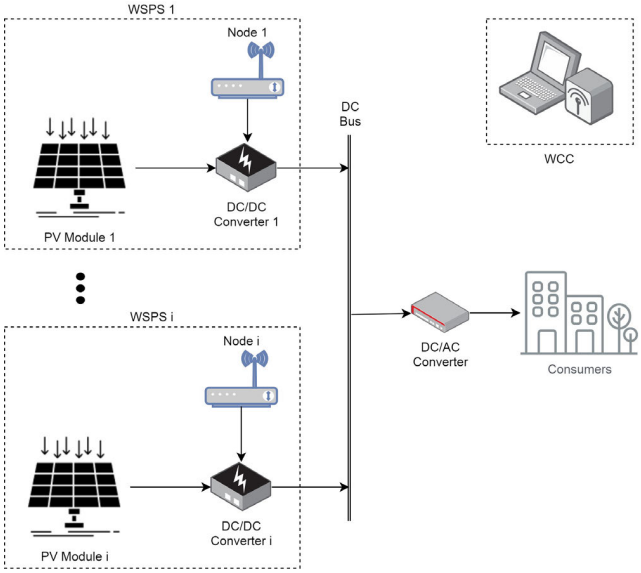

FIGURE 1. Description of the system.

A. WIRELESS SMART PHOTOVOLTAIC SYSTEM

The wsps is made up of one photovoltaic (PV) module, A DC/DC buck-boost converter and a wireless sensor node. In this case, the different wspss are connected to a resistive load, although they can also be connected to a DC/AC converter to transfer power to the electrical network.

1) PHOTOVOLTAIC MODULES

The PV modules used in this work are 20 W_P commercial solar modules with 36 PV cells series connected. Depending on the environmental conditions, such as the irradiance and the temperature that required to be sent to the network node, the pv modules provide a higher or lower power. the maximum power is achieved in the standard conditions with an irradiance of 1000 W/m^2 and a temperature of 25 °C. Table 1 details the electrical features of the used solar modules under these conditions.

The characteristic curves of the PV modules, I-V and P-V, are depicted in Fig. 2 for a range of irradiance and temperature values. Besides, the figure shows the real characteristic curves obtained experimentally, and the simulated curves. The simulated curves were obtained in matlab-simulink using the well-known solar cell model [15]. A comparison between the real and the simulated curves proves the accuracy of the model since both curves give the same values. thus, the voltage that provides the maximum power point and the maximum power could be known under any irradiance and temperature value.

TABLE 1. Electrical parameters of the solar module.

Parameters	Values
Maximum power	20 Wp
Maximum power voltage	17.5 V
Maximum power current	1.15 A
Open-circuit voltage	21.6 V

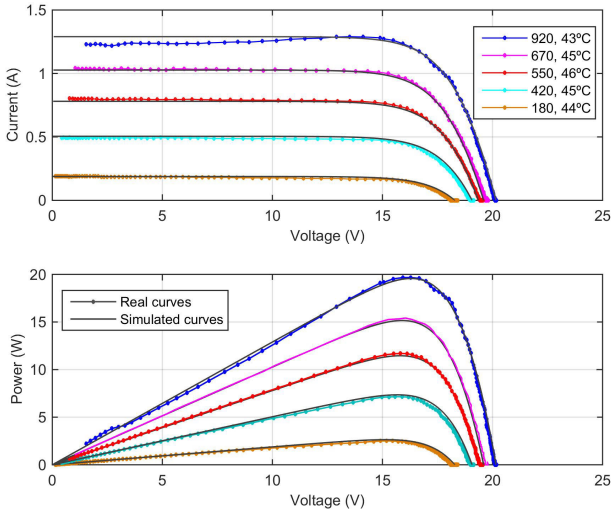

FIGURE 2. I-V and P-V curves of a PV module.

2) DC/DC BUCK-BOOST CONVERTER

The PV module detailed above feeds a built buck-boost converter. Then, in this case, the DC/DC power converter feeds a resistive load of 220 Ω. The buck-boost converter output can also be connected to a DC/AC power converter to transfer energy to the electrical network.

This converter is a DC to DC power converter able to supply an output voltage higher or lower than the input voltage. The value of the output voltage depends on the value of the duty cycle, D. The duty cycle is the ratio of the time when the switch is ON to the total switching period. Thus, the energy transfer from the PV modules to the load is controlled by modifying the duty cycle. The output/input voltage ratio in steady state is (1).

$$\frac{v_o}{v_{in}} = \frac{u}{1-u} \tag{1}$$

The duty cycle is in the interval 0 to 1 and it is controlled by pulse width modulation (PWM).

The buck-boost power converter consists of a filtering capacitor, C_i, in parallel with the PV module's output voltage, with an inductor, L_1, and with another capacitor, C_o. A MOSFET, T, is placed between the input capacitor and the inductor, whereas the diode for loss minimization, D,

is placed between the inductor and the output capacitor in a reverse direction. This converter topology is presented in Fig. 3. i_{L1} is the inductor current, i_{in} is the PV module output current, v_o is the DC/DC converter output voltage.

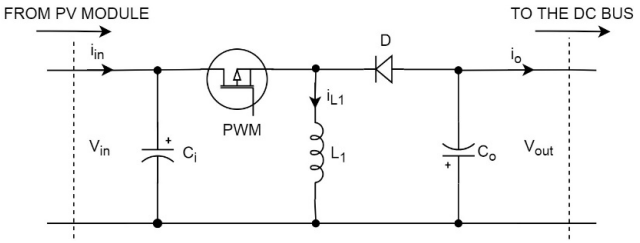

FIGURE 3. Schematic of the buck-boost converter.

The PV modules provide energy to the inductor, where it is stored, when the MOSFET is ON, being the load insulated from the PV array because the diode is inversely polarized. After that, the diode conducts when the MOSFET is open and the energy goes from the inductor to the load. In this case, the buck-boost converter will work in Continuous Conduction Mode (CCM), which means that the inductor current is always positive (never zero) [29]. Thus, during the MOSFET OFF time, the inductor is transferring energy to the load at all times. Besides, it should be noticed that the output voltage has reverse polarity with respect to the buck-boost power converter input voltage.

The use of the MOSFET and the diode makes the DC/DC buck-boost converter behave in a non-linear way. Nevertheless, the equations that model this power converter are the time derivative of the buck-boost converter input voltage (2), the time derivative of the inductor current (3), and the time derivative of the DC/DC converter output voltage (4), by means of the state averaging method.

$$\frac{dv_{in}}{dt} = \frac{i_{in} - ui_{L1}}{C_i} \tag{2}$$

$$\frac{di_{L1}}{dt} = \frac{u(v_{in} + v_o) - v_o}{L_1} \tag{3}$$

$$\frac{dv_o}{dt} = \frac{i_{L1} - ui_{L1}}{C_o} - \frac{v_o}{RC} \tag{4}$$

In this work, the used buck-boost converter is a built one, as shown in Fig. 4. The converter consists of a filtering capacitor with a value of 1000 μF, a 20 mH inductor, an output capacitor with a value of 5700 μF, an MBR10200 diode and a CSD19536KCS MOSFET driven by an FOD3180 driver. The buck-boost converter allows an input voltage between 10 V and 70 V, whereas 100 V is the maximum output voltage. Concerning the power, 70 W is the maximum transfer value. The efficiency of the DC/DC converter is 92% [14]. The output voltage ripple is 0.5% of its value. The buck-boost converter input and output voltages are measured through a voltage divider, whereas the DC/DC converter input and output current and the inductor current are measured by means of a shunt resistor of 0.01 Ω. All these parameters are also sent to the network node to implement the control, although the output current in this case is not required for the control. Fig. 4 shows the WSPS connected to a load.

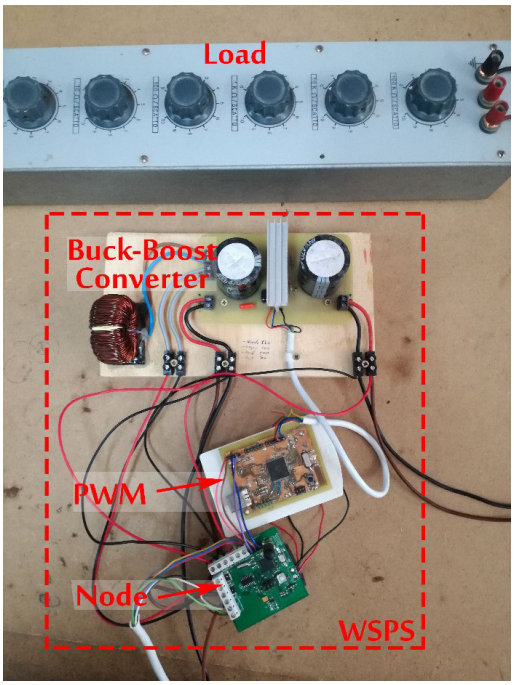

FIGURE 4. Image of the wireless smart photovoltaic system.

The use of the buck-boost converter is due to the fact that it can step up or step down the input voltage level. In PV systems, the boost converter is most frequently used because a higher voltage is typically is needed at the output. If other applications are considered, such as telecommunication applications requiring a voltage between 36 to 75 V [14], or network nodes working at 3.3 V or 5 V [30], to send data in PV plants, the buck-boost converter is a good option to transfer energy (to a load, an inverter or the mentioned apparatus). Then, the buck-boost converter is controlled to achieve the desired voltage. In this case, a MPPT is used to make the PV module work at the voltage that provides the maximum power using non-linear control - the backstepping controller, as it will be presented in Section IV.

3) WIRELESS SENSOR NODE

The developed sensor device allows deploying a wireless network where the gathered data is sent to the coordinator node for further processing in the CTU. The design meets the required small size and low power consumption demands for a wireless node. As the system can be easily scaled up, a low-cost solution is also needed if a high number of sensor nodes are to be deployed. The wireless transmission was used to integrate all independent sensing signals, which allowed for centralization and real-time control.

Fig. 5 shows the hardware building blocks of the developed device. It consists of a microcontroller, a differential analog to digital converter (ADC), a battery, and a set of sensors with analog outputs, which measure the required parameters, i.e., irradiance, current, voltage and temperature. The sensor

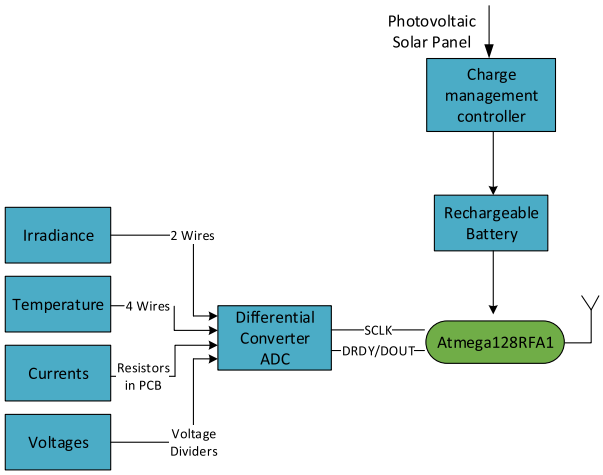

FIGURE 5. Building blocks of the sensor node.

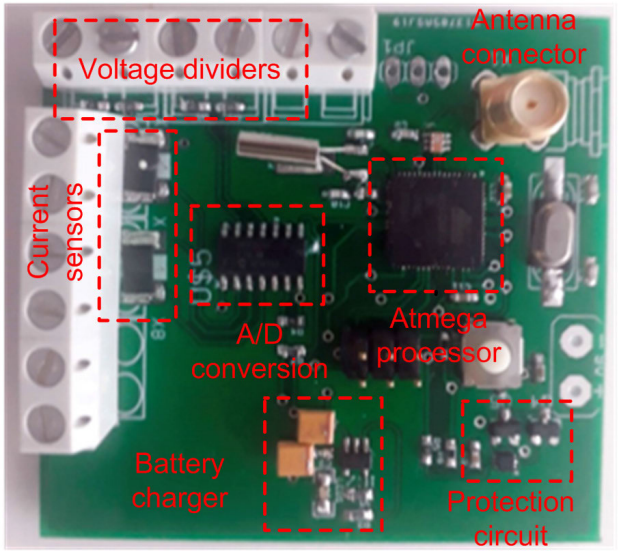

FIGURE 6. Photograph of the wireless sensor node.

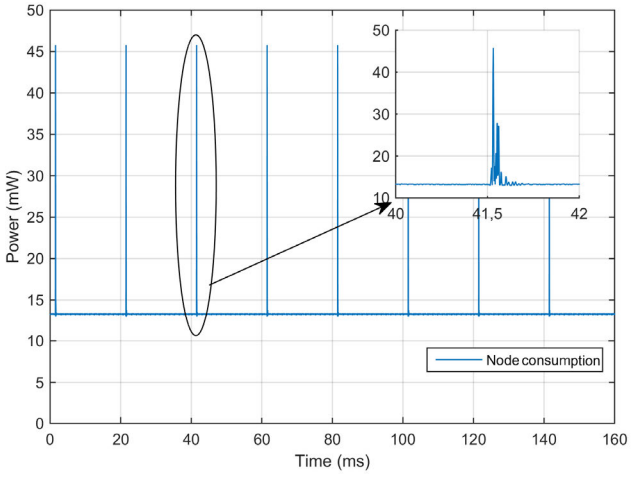

FIGURE 7. Measured power consumption of the sensor node.

node is powered by a battery, but the autonomy is guaranteed by operating from the PV modules.

The 8-bit ATmega128RFA1 microcontroller from Atmel is a low power device combined with a high data rate transceiver for the 2.4 GHz ISM band, fully compatible with ZigBee and IEEE 802.15.4 standards. The radio transceiver requires a minimum number of external components, reducing costs and size requirements. Furthermore, it features robust, high data rates wireless communication capabilities, combined with low current consumption. The microcontroller must handle the communication stack of the IEEE 802.15.4 standard. In order to reduce the microcontroller load and improve the software management to achieve real time monitoring, an external analog to digital converter has been included to sample the sensors. The MCP3428 from Microchip is a 16-bit ADC with four-channel differential inputs. This large precision ensures a minimum measured current of 9 μA, which is sufficient for the control of the DC/DC buck-boost converter. Moreover, this ADC has been chosen because it can be put in a low-power standby mode or shut down completely in its power-down mode through simple pin-driven control. The data from the ADC is directly transferred to the microcontroller (SPI bus). Fig. 6 shows the board of the sensor node.

Fig. 7 shows the power consumption of the sensor node measured in the laboratory. It is observed that it needs an average consumption of 13.28 mW and for the transmission of the data it presents a consumption of 46.11 mW. In the worst case, this represents only 0.25% of the power delivered by the photovoltaic module.

B. WIRELESS CENTRALIZED CONTROL

The WCC is divided in two parts, the CTU and the coordinator (host) node. The MPPT and the backstepping control form the CTU. The coordinator node receives all the data sent by the PV system (irradiance, temperature, PV output voltage and current, DC/DC converter output voltage and current, and the inductor current) and communicates with the CTU.

1) COORDINATOR NODE

The connection between the coordinator node and the monitoring computer, where the data is assessed and processed, is done through USB. The data from the sensor nodes is gathered by the coordinator (host) node, which transmits it to the monitoring application in charge of handling the network. Fig. 8 shows an image of the wireless centralized control.

The coordinator node is governed by the 8-bit ATmega128RFA1 microcontroller and sends data by serial communication to the control terminal unit (CTU) (implemented by a RaspBerry Pi). Just like in the sensor node, an antenna connected through an SMA connector has been implemented. The coordinator node is fed from an external power supply via pin or jag connector.

2) MPPT & BACKSTEPPING CONTROL

The backstepping control, which will be explained later, regulates the buck-boost converter input voltage to make the

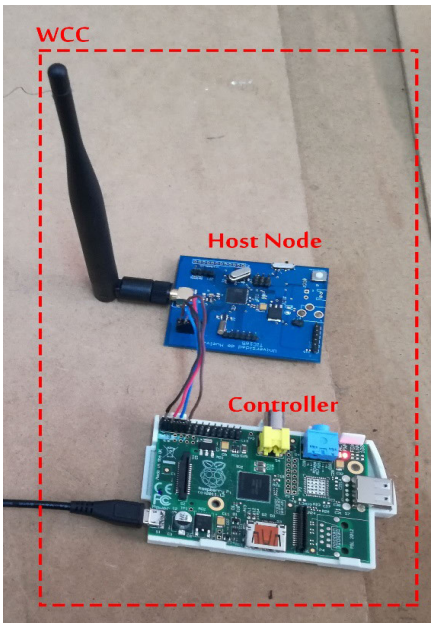

FIGURE 8. Photograph of the Wireless Centralized Control: wireless coordinator (host) node and controller (CTU).

PV modules track the voltage that provides the maximum power, by means of the duty cycle control. The voltage to work in the maximum power point (MPP) is previously calculated for different environmental conditions by means of a regression plane adjusted with a modified perturb and observe (P&O) algorithm [15]. The modified P&O provides an incremental value of the reference voltage, $\Delta v_{ref,p}$, instead of the duty cycle value. As such, the final reference voltage that enforces the system to work at the maximum power point is obtained by the addition of the theoretical reference voltage, $v_{ref,t}$, and the incremental voltage, as Fig. 9 shows. This method reaches the global maximum, avoiding the local ones. Thus, the regression plane together with the modified P&O is used by the backstepping control as initial reference for the voltage, $v_{ref,f}$.

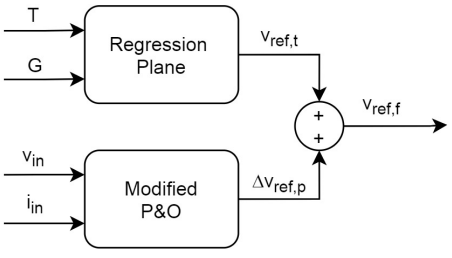

FIGURE 9. MPPT algorithm diagram.

III. PERFORMANCE OF THE WIRELESS COMMUNICATION

The IEEE 802.15.4 standard sets two mechanisms to synchronize the transmission of information: non beacon-enabled mode and beacon-enabled mode. The beacon-enabled mode is based on the continuous monitoring of beacons by nodes associated to the transmitter of such beacons (coordinator node). It uses a structure for the data transfer known as superframe, where a guaranteed time slot (GTS) mechanism can achieve a fixed data monitoring latency with an adjustable sample period. Thus, as the target application requires low latency, each sensor node can use previously defined portions of the active superframe (GTS) for the data transmission to the coordinator node. The access of the nodes to the medium is determined by a slotted CSMA/CA (Carrier Sense Multiple Access with Collision Avoidance) mechanism synchronized by means of the beacons of this structure [31]. Therefore, the use of the IEEE 802.15.4 standard in beacon-enabled mode allows synchronization between the sensor nodes and the coordinator node and ensures the correct transmission of data between them.

We have estimated that the controller for the DC/DC converter performs stably if it receives data at time intervals of less than 20 ms. In order to achieve this objective, the information transmission times in the IEEE 802.15.4 standard have been configured by BO (macBeaconOrder) and SO (macSuperframeOrder) parameters [32]: for BO=SO=0, the time interval between the sending of each beacon is 15.36 ms. Therefore, this is the duration of a superframe that contains the information of the data acquired by the sensors. Furthermore, the flight time of the information must also be taken into account, and thus it has been measured using a sniffer. The measurements in Fig. 10 show that the flight time is less than 4.5 ms. Therefore, the total transmission time of the information from the sensor node to the coordinator node will allow the controller to perform properly.

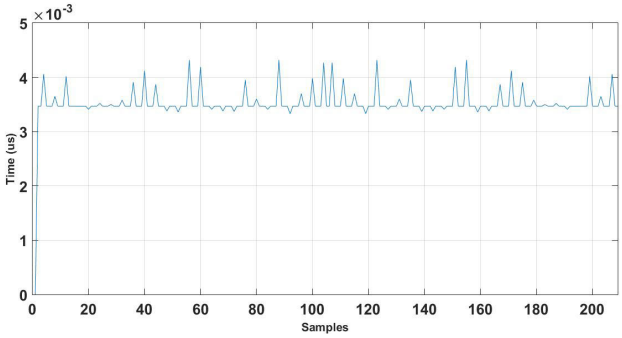

FIGURE 10. Measured flight time of the data transmission.

A. FIRMWARE

The IEEE 802.15.4 standard ensures reliability with the association of the sensor nodes to the coordinator node of the network. The coordinator node is responsible for managing the network and assigning the addresses to the sensor nodes. Fig. 11 shows the negotiation protocol for the initial association in beacon-enabled mode. When the non-associated node begins the association, first it transmits an association request that must be accepted by the coordinator node. Afterwards, the requesting node asks for an answer to the association request. If it is successful, it receives the association data,

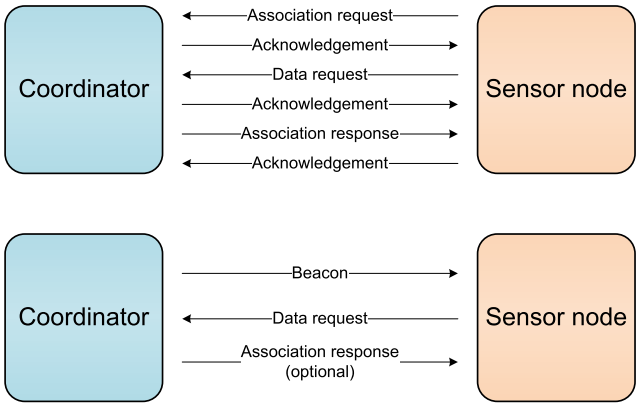

FIGURE 11. Association protocol for IEEE 802.15.4 beacon.

which it must confirm with an acknowledgment (ACK) frame.

The use of the CSMA/CA mechanism does not ensure that a transmission can take place within a superframe corresponding to that monitoring instant, since the mechanism provides media access where each sensor node randomly selects a time slot to transmit. However, if the transmission cannot be completed, this will be done in the CAP (contention access period) area of the next superframe. This fact results in time delays that may affect the stability of the controller. Therefore, sensor nodes overcome this problem by using the guaranteed time slot (GTS) mechanism to provide data monitoring with a predetermined latency. It consists of time slots within each superframe, which are allocated by the coordinator node to each sensor node. Thus, the data transmission is guaranteed within each superframe and the periodicity of the transaction is fixed, ensuring the proper performance of the controller.

Each sensor node collects the PV module parameters and a GTS is reserved for the transmission of data. The communication from the sensor node towards the coordinator node is as follows: the coordinator sends a beacon and the sensor node waits until the instant fixed in the GTS to transmit the data; the proper reception is confirmed by an acknowledgment of the coordinator. This data is processed by the control terminal unit (CTU) of the WCC, which returns to the sensor node the control parameter for the DC/DC converter to track the MPPT. This transmission from the coordinator to the sensor node is set by the IEEE 802.15.4 standard as follows: the coordinator sends a beacon, followed by a request of data from the sensor node. Then, the coordinator node sends an acknowledgment followed by the data, and the sensor node ends the transmission with another acknowledgment.

As described above, both the sensor nodes and the coordinator node are governed by microcontrollers from Atmel. The Atmel MAC (Media Access Control) architecture follows a layered approach based on several stack modules that allow establishing the mechanisms and functionality of the IEEE 802.15.4 standard for the wireless transceivers. Among them, the modules that have been adapted to the target application requirements are the followings:

- Platform Abstraction Layer (PAL): provides interfaces to timers, GPIO control (access from microcontroller to the general purpose I/O pins connected to the transceiver), low-level interrupt handling, serial I/O support and access to storage.
- The MAC module: includes the protocol stack of the 802.15.4 communications standard; within this module we must highlight MAC-API, which is the stack for specific applications;
- TAL: contains the transceiver specific functionality.
- Resources: includes the management of buffers and the queues.

The above modules have been used for both the coordinator node and sensor nodes.

Programming the coordinator begins with the configuration of a number of parameters, amongst which are Beacon Order (BO), Superframe Order (SO), channel, or network name. The time between beacons and the time when the sensor node can transmit are determined from the parameters BO and SO, which are defined by the standard.

The network coordinator is responsible for setting up the wireless network and launching the beacons to receive the data sent by the sensor nodes. The flowcharts of the network coordinator and the end devices are shown in Fig. 12. In Fig. 12(a) is shown the flow chart of the coordinator node. The first action taken is the configuration of the parameters required to create the network, after which the coordinator waits to receive a beacon from any of the sensor nodes. Upon receiving the first broadcast (that is, a sensor node has sent an association beacon), the coordinator associates a PV module number to the MAC address of the sensor node, then broadcasts an association beacon and waits for the sensor node to respond. Upon receiving the association

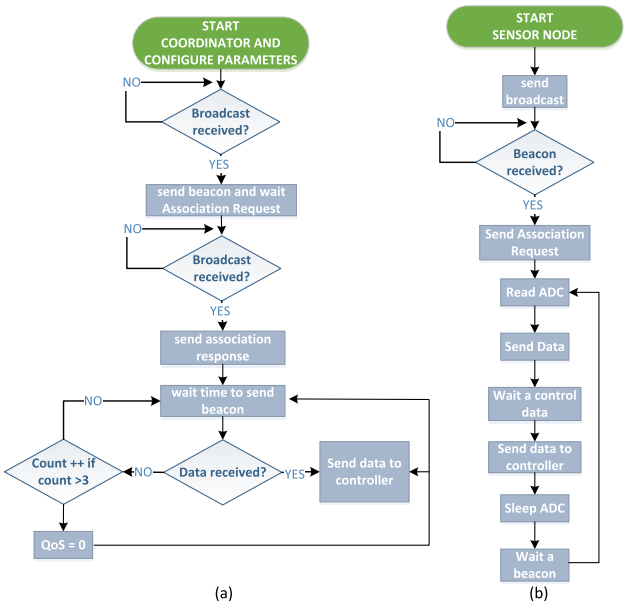

FIGURE 12. (a) Flow chart of the coordinator node. (b) Flow chart of the sensor nodes.

agreement confirmation from the sensor, the address of the latter is already in the buffer of the coordinator. In the next step, the coordinator sends a data request beacon after waiting for a period defined by the BO and SO parameters. Once the beacon is sent, either of the two following cases can occur: the coordinator can receive the acknowledgement from the sensor node, in which case the data is sent to the base station given that the sensor node is already associated; or, on the contrary, no data is received by the coordinator, in which case is sends another beacon. A number of three attempts are programmed in the protocol stack for the latter case, after which the coordinator informs the base station of this situation by sending the data QoS $= 0$.

In Fig. 12(b) appears the flow chart corresponding to the sensor nodes. The first action taken by the sensor node is to try and associate to the network by sending an association frame, also known as broadcast (it is defined as association beacon within the standard). Upon receiving the response from the coordinator, the association is accepted by the sensor node. Next, the sensor node wakes the ADC from its sleep mode and takes a data reading. The data is then sent to the coordinator node, and the ADC is again put in sleep mode to reduce power consumption. After successfully sending the data to the coordinator node, the sensor node waits to receive a new beacon in order to repeat the above procedure.

IV. CONTROL SYSTEM

The backstepping control method is used as an effective approach to design controllers for a large class of nonlinear systems [14]. This way, all the dynamics of the system are taken into consideration when the controller is designed. Then, the working is better compared with a linearized system since the controlled system works appropriately regardless the point where is located at all times. The backstepping control uses a recursive procedure to model direct dynamics taking into account the uncertain bounded nonlinearities and uncertainties in the parameters. For that, intermediate virtual control laws are created using Lyapunov functions to guarantee that the system is robust under abrupt variations, stable, and it has a computable transient response. Thus, it starts from a lower order system and increases the order with new dynamics, obtaining a recursively defined composite Lyapunov function. The Lyapunov functions are globally positive-definite and the system will be globally asymptotically stable if the time derivatives of the Lyapunov functions are negative. The states of the system must be stabilized towards the origin (zero error), being the origin the equilibrium point.

In this work, the plant we use to apply the backstepping control to is the buck-boost converter, which is modeled by eq. (2) to (4). The DC/DC converter controls the PV module's output voltage. The objective of the controller is to regulate the DC/DC converter input voltage (the PV module output voltage) to guarantee the PV modules work at the maximum power point by means of the control of the duty cycle of the buck-boost converter. Thus, the maximum power extraction is ensured. The reference voltage that is tracked is the voltage that provides the maximum power, which is obtained by means of the regression plane explained before.

To achieve the tracking of the voltage that supplies the maximum power point using the backstepping method, the design procedure is to obtain an inner current control loop to control the inductor current, i_{L1}, (by defining the buck-boost converter duty cycle, u, recursively) and then an outer voltage loop controls the PV modules output voltage, v_{in}, generating the inductor reference current used by the inner loop. The steps of the backstepping controller are explained as follows, taking into consideration equations (2) and (3).

The first step is to define the voltage error as the difference between the input voltage and the reference voltage, v_{in}^r, to make the buck-boost converter input voltage track the reference voltage that provides the maximum power point. Thus, the aim is to obtain a zero error to stabilize the DC/DC converter at the origin. Then, the time derivative of the voltage error (5) is obtained using (2).

$$\frac{de_v}{dt} = \frac{i_{in} - u i_{L1}}{\mathrm{C_i}} - \frac{dv_{in}^r}{dt} \tag{5}$$

In the time derivative of the voltage error, i_{L1} is the virtual control law and the current reference. Thus, it has to be calculated later.

The next step is to define a globally positive definite and radially unbounded for all e_v Lyapunov function. Besides, the time derivative of the Lyapunov function is negative definite for all e_v to guarantee a local asymptotic stability. The selected Lyapunov function and its time derivative are presented in (6) and (7), taking into account (5).

$$V_v = \frac{1}{2} e_v^2 \tag{6}$$

$$\frac{dV_v}{dt} = \frac{i_{in} - u i_{L1}}{\mathrm{C_i}} e_v - \frac{dv_{in}^r}{dt} e_v = -\mathrm{k_v} e_v \tag{7}$$

where k_v is a positive gain to enforce $dV_v/dt < 0$.

Now, the inductor reference current is worked out from (7). Thus, the stabilization function is obtained, taking into account that $0 < u < 1$ and $\alpha = i_{L1}$.

$$\alpha = \frac{\mathrm{C_i k_v} e_v + i_{in} - \mathrm{C_i} \frac{dv_{in}^r}{dt}}{u} \tag{8}$$

The stabilization function is a function to define the duty cycle of the DC/DC converter. For that, it is required a second feedback loop and a current error is defined, e_{iL}, as the difference between the inductor current and the stabilization function, to make the inductor current track the inductor reference current (α) and make the error disappear [14].

To calculate the time derivative of the current error it is required to obtain previously the time derivative of the stabilization function, considering that the inductor current i_{L1} is replaced by $e_{iL} + \alpha$. Then, the time derivative of the current

error is calculated in (9).

$$\frac{de_{iL}}{dt} = \frac{v_o + (v_{in} - v_o)u}{L_1} - (k_v e_{iL} - \frac{C_i k_v^2}{u} e_v - \frac{C_i}{u}\frac{d^2 v_{in}^r}{dt^2} + \frac{1}{u}\frac{di_{in}}{dt} - \frac{\alpha}{u}\frac{du}{dt}) \quad (9)$$

The next step is to choose another Lyapunov function with similar properties to (6). V_v has to be included in the inductor current Lyapunov function, which is composed in a recursive way.

$$V_i = V_v + \frac{1}{2} e_{iL}^2 \quad (10)$$

The time derivative of this new Lyapunov function is obtained in (11) taking into account the time derivative of the voltage error, the time derivative of the current error (9), and replacing the inductor current i_{L1} by $e_{iL} + \alpha$.

$$\frac{dV_i}{dt} = -k_v e_v^2 + e_{iL}[\frac{v_o + (v_{in} - v_o)u}{L_i} + e_v(\frac{C_i k_v^2}{u} - \frac{u}{C_i}) - k_v e_{iL} + \frac{C_i}{u}\frac{d^2 v_{in}^r}{dt^2} - \frac{1}{u}\frac{di_{in}}{dt} + \frac{\alpha}{u}\frac{du}{dt}] = -k_v e_v^2 - k_i e_{iL}^2 \quad (11)$$

As before, the parameters k_v and k_i are positive gains to enforce that the time derivative of V_i is negative and thus guarantee the stability of the system. To obtain the time derivative of the duty cycle in order to control the buck-boost converter, it is required that $-k_i e_{iL}^2$ be equal to the term between square brackets that is accompanying e_{iL}. Then, working out the value of the time derivative of the duty cycle, equation (12) is obtained.

$$\frac{du}{dt} = \frac{1}{\alpha}[\frac{-v_o u - (v_{in} - v_o)u^2}{L_i} - e_v(C_i k_v^2 - \frac{u^2}{C_i}) + e_{iL}(k_v - k_i)u - C_i\frac{d^2 v_{in}^r}{dt^2} + \frac{di_{in}}{dt} \quad (12)$$

where the duty cycle satisfies $0 < u < 1$ and the stabilization function α is different from zero.

Finally, equation (12) has to be integrated to obtain the duty cycle of the buck-boost converter in order to control the PV modules output voltage to obtain the maximum power.

Fig. 13 summarizes the backstepping control. As it was explained before, the backstepping uses a recursive methodology that steps backwards until the final control signal is obtained. There are two control loops. One control loop includes the voltage error (known as the virtual control signal) and α is obtained. Another control loop includes the current error. Then, the time derivative of the duty cycle is obtained, and it has to be integrated to control the buck-boost converter.

Once the entire control system has been described in detail, the overview shown in Fig. 14 summarizes how the signals are sent and received in the system. The ADC converter of the WSPS samples all the signals provided by the sensors at a

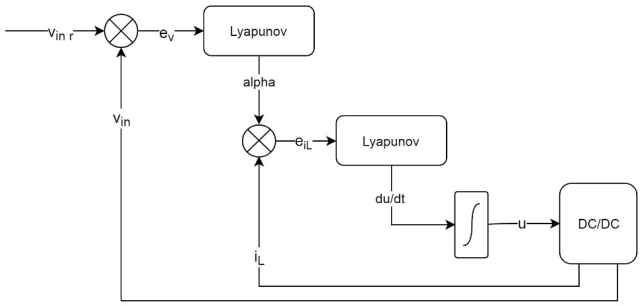

FIGURE 13. Backstepping control diagram.

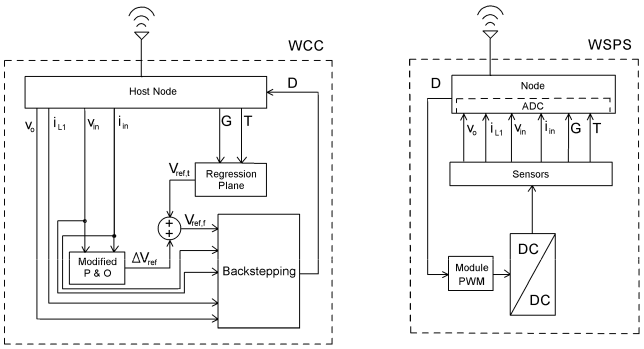

FIGURE 14. Overview of the signal flow in the wireless remote control scheme.

frequency of 100 Hz. Then, these signals are sent to the WCC through the transmission module with a frequency of 100 Hz using the 802.15.4 protocol. Besides, the WSPS receives the control signal generated by the WCC and transfers it to the PWM module to control the DC/DC converter. The data received in the coordinator node from the WSPS is sent through serial communication to the CTU. The implementations of the MPPT and the backstepping control previously explained are in the CTU. The sampling time of the controller is 10 ms. The controller gains, k_v and k_i, have been obtained empirically and their values are 5 and 75, respectively.

V. EXPERIMENTAL RESULTS

A. FIELD TEST OF THE WIRELESS COMMUNICATION RELIABILITY

The DC/DC converters work with a lot of power and generate hard-to-control magnetic fields, which in this application can affect the wireless transmission of data between the sensor nodes and the coordinating node. For this, experimental measurements of noise and LQI (Link Quality Indicator) have been carried out under different working conditions of the DC/DC converter, which will allow to determine the most appropriate communications band of the IEEE 802.15.4 standard for this application. The tests have been carried out in the 2.4 GHz band. It should be clarified that, although the radio frequency signal losses are measured in dBm, in the following graphs the results have been represented in percentages, since in this way the measurements of power and quality of the signal can be included in the same graph.

The experimental setup has been the same in all the tests performed: a sensor node sends data to a coordinating node located near the converter, and a sniffer node, based on the MC1322X microcontroller, reads all the network information. This node studies the quality of the signal in the air, which is used to see the signal losses during the various experiments. Fig. 15 shows the results when the DC/DC converter is stopped. The initial drop in the signal is due to the 20 m distance that separates the nodes.

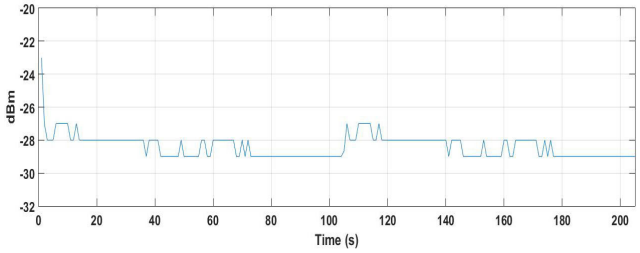

FIGURE 15. Background noise without influential magnetic fields.

Next, the converter has been put into operation, with its power stepwise increased to a maximum of 40 W, as shown in the red line of Fig. 16. The blue line, as in the previous graph, represents the quality of the signal measured by the sniffer. It can be seen how as the output power of the converter increases; the signal quality decreases only slightly. Therefore, it is concluded that the wireless data transmission can be performed with complete reliability.

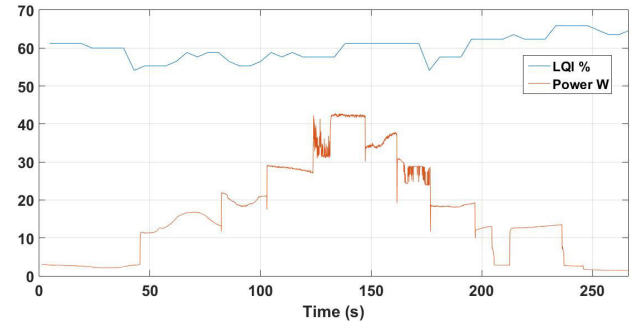

FIGURE 16. Influence of the magnetic fields generated by the converter.

Finally, in Fig. 17 there can be observed the difference in signal quality when the converter is running and when the converter is turned off. The red line represents the background noise, that is, the measurement without any converter running, and the blue line represents the signal losses when the converter is running. The existence of losses can be observed, but it is concluded that they are not significant enough as to prevent the wireless communication from being established.

B. MONITORING APPLICATION

The monitoring application is designed in Visual Basic. The data read by the different sensors is sent to the base station. The data can be processed, analysed and finally visualized

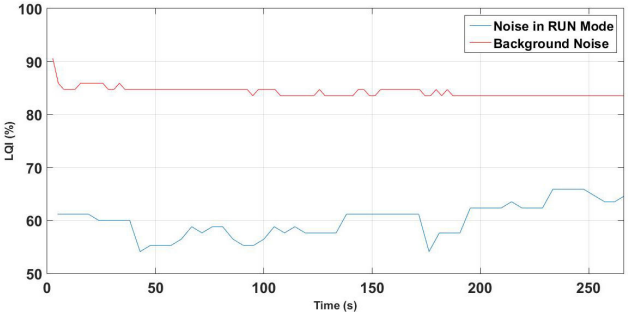

FIGURE 17. Difference in percentages between background noise with, and without the converter running.

through different displays that show the values numerically or graphically. The application allows to save the experiment data in a file with.txt extension. Thus, the data is available to be used later. The values obtained from the sensors are the DC/DC converter input and output voltage, the inductor current, and the buck-boost converter input and output current. Besides, the duty cycle is also visible from the application.

Fig. 18 presents a screenshot capture of the graphical user interface (GUI). As it is shown, there are different tabs to interact with the application. One of the tabs provides the options to adjust the sensors and set their maximum allowable values. In addition, the parameters of the controller can also be adjusted. In another tab, the operating mode of the backstepping controller can be changed from automatic to manual in the case there is any problem with the supply. Besides, the GUI shows in real time the values of the sensors.

C. LABORATORY EXPERIMENTAL SETUP AND FIELD TESTS

To validate the proposed remote controller using wireless communication, an experimental setup has been designed. Then, the experiments have been carried out under different weather conditions. The PV modules, the buck-boost converter and the nodes have been presented in Section II.

The buck-boost hardware is connected directly to the sensing node and to the PWM generator. The node will measure the values of the irradiance, temperature, inductor current and voltage, and current at the output and input of the converter. The data from the sensors is received wirelessly by the coordinator node and sent to the CTU. Then, the PWM signal is generated at the desired frequency. The control signal is generated by the CTU and then it is sent to the buck-boost converter. The switching frequency noise is removed using a low-pass filter. The CTU with a virtual instrument is required to supervise the experiments via wireless communication. The program is implemented with Visual Basic using C language, and the integrated development environment is MPLAB. The features of the controller programming are presented in Table 2.

The system has been tested under dynamic weather conditions since the irradiance and the temperature will take

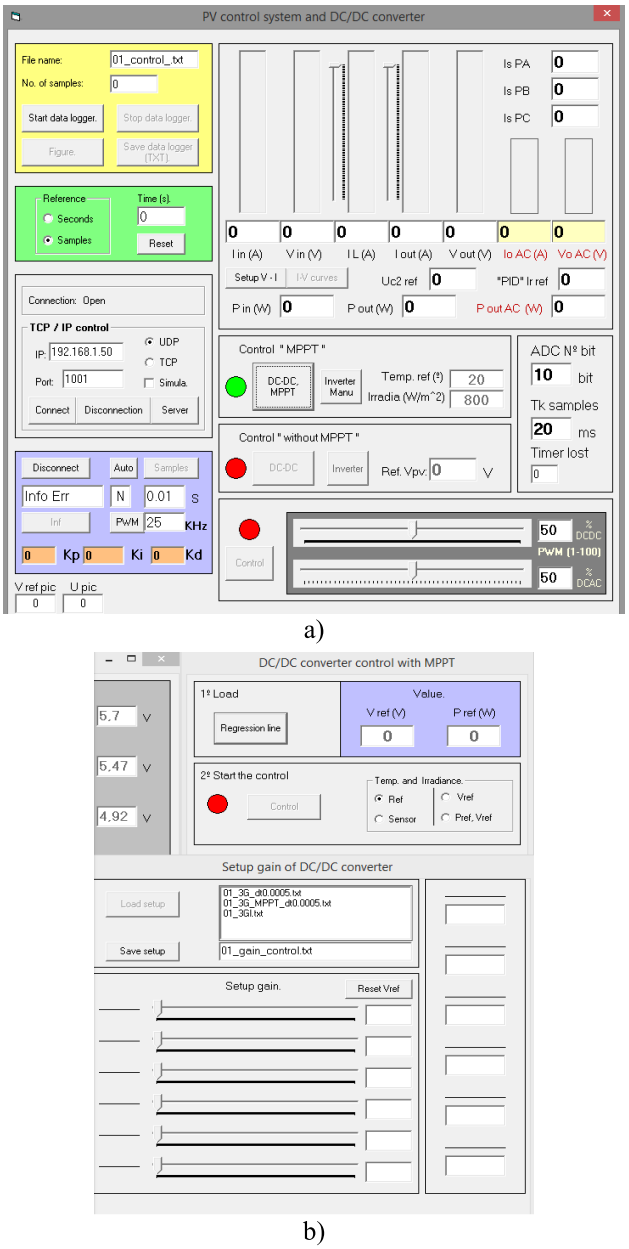

a)

b)

FIGURE 18. Graphical user interface in Visual Basic a) PV control system and DC/DC converter b) DC/DC converter control with MPPT.

TABLE 2. Features of the controller programming.

PWM frequency	25 kHz
Resolution of the PWM	10 bits
Sampling time of the backstepping control loop	10 ms
Duty cycle change rate	10 ms

different values. Fig. 19 depicts the changes of the environmental conditions. First, the irradiance has a value of 693 W/m^2 and the temperature is 37 °C. The temperature undergoes little changes (about 1°C) while the irradiance

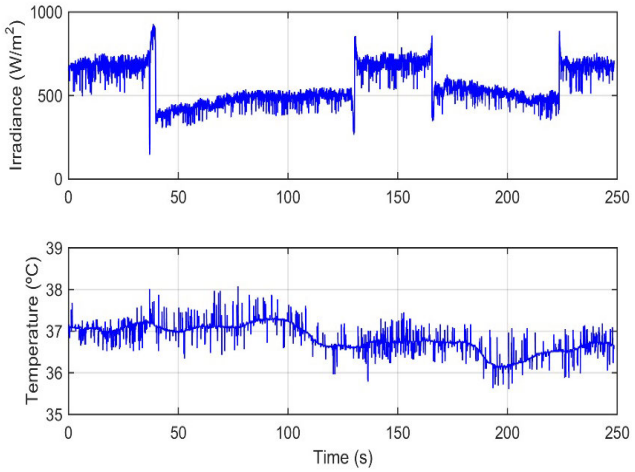

FIGURE 19. Irradiance and temperature changes.

TABLE 3. Values at the maximum power point.

Time (s)	Irradiance (W/m^2)	Temperature (ºC)	v_{ref} (V)	P_{MPP} (W)
[0-39)	693	37.1	16.2	17.9
[39-131)	495	37.3	15.2	7.2
[131-166)	687	36.7	16.2	18
[166-224)	525	36.2	15.5	8.1
[224-250]	680	36.6	16.2	17.9

drops from 693 W/m^2 to 495 W/m^2 approximately, then it increases very fast to 687 W/m^2 to drop again to 525 W/m^2. Finally, the irradiance increases rapidly again to 680 W/m^2.

For each value of irradiance and temperature there is a value of the voltage that provides the maximum power point. Table 3 presents the time, irradiance, temperature, and voltage that supply de maximum power, and the MPP values.

Fig. 20 shows the voltage results obtained under the irradiance and temperature described in Table 3. It presents the reference voltage that has to be reached to achieve the maximum power, and the DC/DC converter input and output voltage.

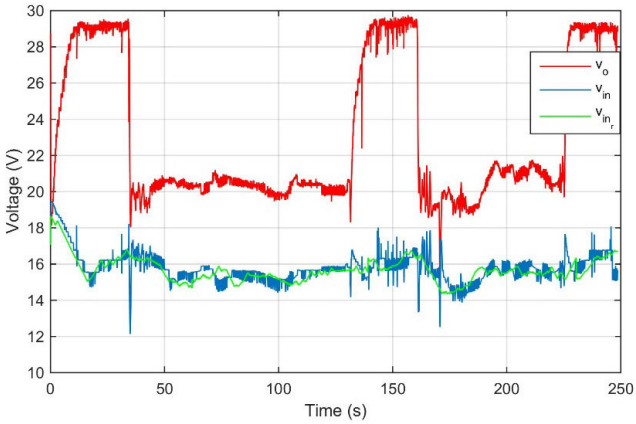

FIGURE 20. Reference voltage, DC/DC converter input and output voltage.

The buck-boost converter output voltage increases when the irradiance rises, and it drops when the irradiance raises as well and the voltage drops when the irradiance decreases. Besides it is shown that the array voltage tracks correctly the reference voltage since the measured signal at the DC/DC converter input matches the reference signal very well, guaranteeing the maximum power extraction.

Then, the results confirmed that the remote control works successfully because the tracking efficiency, which it is defined as the ratio between the array voltage and the reference voltage, is over 99% even in the presence of variable climatic conditions. Thus, the controller can regulate the buck-boost converter input voltage reaching the MPP for each irradiance and temperature.

Next, the current signals flowing through the DC/DC converter are presented in Fig. 21.

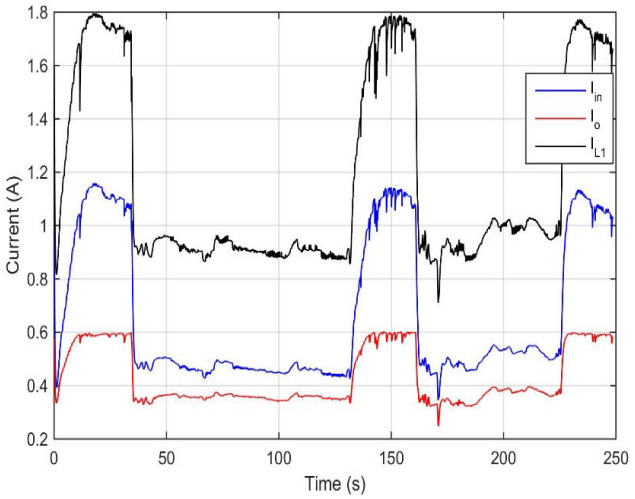

FIGURE 21. Inductor current, DC/DC converter input and output current.

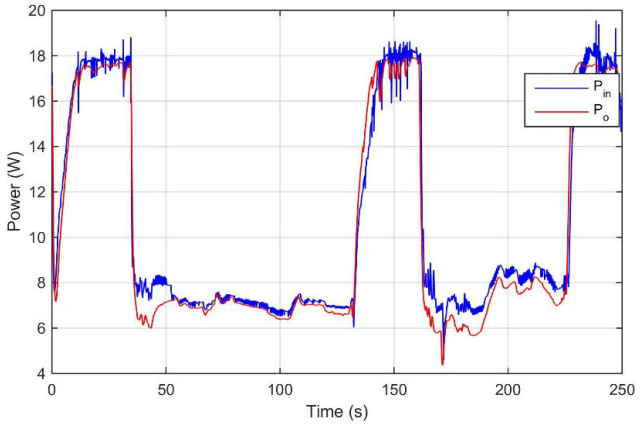

FIGURE 22. DC/DC converter input and output power.

The behavior of the signals is similar to the buck-boost output voltage, with the currents increasing when the irradiance rises and decreasing when the irradiance drops. The effect of the temperature is also presented. It is easily seen at around 200 s that the output current and voltage slightly increase when the temperature drops about 1°C.

Fig. 22 depicts the power extracted from the PV system (the input power) and the power transferred to the load (the output power).

The buck-boost converter input power matches the maximum power thanks to the performance of the remote controller. As it is commented previously, the reference tracking is higher than 99%. These results also show the DC/DC converter efficiency. The output power is lower than the input power due to the switching losses and the parasitic resistance of the inductor. As a result, the transferred energy is between 92% and 98% of the input energy.

Finally, Fig. 23 presents the control signal. It shows the behavior of the controller when the irradiance and the temperature change.

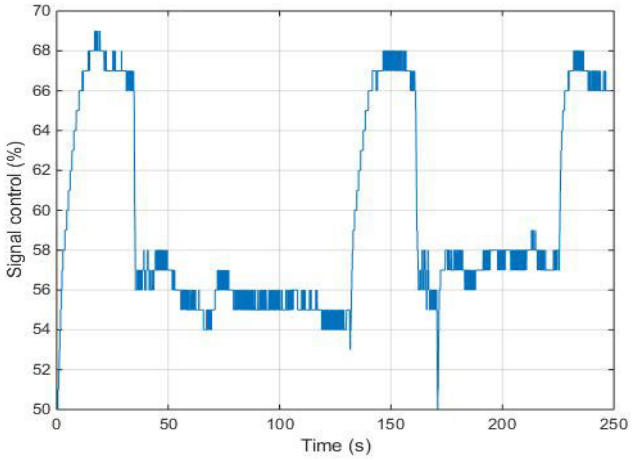

FIGURE 23. Control signal.

The results have confirmed the robustness of the controller under parameter variations. It also considers the worsening in the buck-boost converter electronic components. Besides, the remote control has an appropriate behavior and the system does not have oscillations, remaining stable even with step changes in the irradiance.

VI. DISCUSSION AND CONCLUSIONS

The popularity of wireless technologies has motivated the trend to design wireless networks for control and monitoring applications. In this context, this work proposes to show the validity of the maximum power point tracking algorithm and the DC/DC converter backstepping control using wireless communication. Wireless sensor nodes using IEEE 802.15.4 technology sense the photovoltaic operation and send the required parameters to a coordinator node to monitor and control the PV system remotely.

A priority issue in the design of the wireless real-time monitoring and control system is to ensure that the controller receives the data correctly within a specified time. To address this matter, a custom WSN has been designed, which operates in beacon enable mode and makes use of the GTS mechanism,

where the coordinator node guarantees that each sensor node has a certain time to send the data. Moreover, the access of the sensor nodes to the medium is determined by a slotted CSMA/CA mechanism synchronized by means of the beacons. Therefore, the use of the IEEE 802.15.4 standard in beacon-enabled mode allows synchronization and the correct transmission of data between the sensor nodes and the coordinator node with low latency, ensuring a stable performance of the backstepping controller.

Experimental measurements confirm the suitability of the deployed wireless sensor network and the usefulness to track the MPP in real-time, maximizing the generation, with an efficiency between 99.02% and 99.98%. Thus, the system is not affected by the wireless communication and the power reached by the MPPT is the maximum power point under any environmental condition. Besides, the DC/DC converter efficiency ranges between 92% and 98%. A reliability test of the wireless communication in the 2.4 GHz band was carried out showing that the noise generated by the operation of the DC/DC converter does not affect the wireless communications.

The deployed system fulfills some mandatory properties in wireless sensor networks: compact design, low power consumption, low cost, robustness against interference and security, thus providing a wide application prospect. It can be easily scaled up, including other sensors on the sensing node to measure other parameters of interest, or adding new sensing nodes to the wireless network.

REFERENCES

[1] L. Xu, W. He, and S. Li, "Internet of Things in industries: A survey," *IEEE Trans. Ind. Informat.*, vol. 10, no. 4, pp. 2233–2243, Jan. 2014.
[2] M. García-Castellano, J. M. González-Romo, J. A. Gómez-Galán, J. P. García-Martín, A. Torralba, and V. Pérez-Mira, "ITERL: A wireless adaptive system for efficient road lighting," *Sensors*, vol. 19, no. 23, p. 5101, Nov. 2019.
[3] N. M. Nor, A. Ali, T. Ibrahim, and M. F. Romlie, "Battery storage for the utility-scale distributed photovoltaic generations," *IEEE Access*, vol. 6, pp. 1137–1154, 2018.
[4] M. Balato, L. Costanzo, and M. Vitelli, "DMPPT PV system: Modelling and control techniques," in *Proc. Adv. Renew. Energies Power Technol.*, vol. 1, 2018, pp. 163–205.
[5] K. A. K. Niazi, Y. Yang, and D. Sera, "Review of mismatch mitigation techniques for PV modules," *IET Renew. Power Gener.*, vol. 13, no. 12, pp. 2035–2050, Sep. 2019.
[6] D. Verma, S. Nema, A. M. Shandilya, and S. K. Dash, "Maximum power point tracking (MPPT) techniques: Recapitulation in solar photovoltaic systems," *Renew. Sustain. Energy Rev.*, vol. 54, pp. 1018–1034, Feb. 2016.
[7] S. Lyden and M. E. Haque, "Maximum power point tracking techniques for photovoltaic systems: A comprehensive review and comparative analysis," *Renew. Sustain. Energy Rev.*, vol. 52, pp. 1504–1518, Dec. 2015.
[8] M. Killi and S. Samanta, "Modified perturb and observe MPPT algorithm for drift avoidance in photovoltaic systems," *IEEE Trans. Ind. Electron.*, vol. 62, no. 9, pp. 5549–5559, Sep. 2015.
[9] M. Alsumiri, "Residual incremental conductance based nonparametric MPPT control for solar photovoltaic energy conversion system," *IEEE Access*, vol. 7, pp. 87901–87906, 2019.
[10] C. Barth and R. C. N. Pilawa-Podgurski, "Dithering digital ripple correlation control for photovoltaic maximum power point tracking," *IEEE Trans. Power Electron.*, vol. 30, no. 8, pp. 4548–4559, Aug. 2015.
[11] H. Rezk, M. Aly, M. Al-Dhaifallah, and M. Shoyama, "Design and hardware implementation of new adaptive fuzzy logic-based MPPT control method for photovoltaic applications," *IEEE Access*, vol. 7, pp. 106427–106438, 2019.
[12] S. Padmanaban, N. Priyadarshi, M. S. Bhaskar, J. B. Holm-Nielsen, V. K. Ramachandaramurthy, and E. Hossain, "A hybrid ANFIS-ABC based MPPT controller for PV system with anti-islanding grid protection: Experimental realization," *IEEE Access*, vol. 7, pp. 103377–103389, 2019.
[13] H. Li, D. Yang, W. Su, J. Lu, and X. Yu, "An overall distribution particle swarm optimization MPPT algorithm for photovoltaic system under partial shading," *IEEE Trans. Ind. Electron.*, vol. 66, no. 1, pp. 265–275, Jan. 2019.
[14] A. D. Martin, J. M. Cano, J. F. A. Silva, and J. R. Vazquez, "Backstepping control of smart grid-connected distributed photovoltaic power supplies for telecom equipment," *IEEE Trans. Energy Convers.*, vol. 30, no. 4, pp. 1496–1504, Dec. 2015.
[15] A. D. Martin and J. R. Vazquez, "Backstepping controller design to track maximum power in photovoltaic systems," *Automatika*, vol. 55, no. 1, pp. 22–31, Jan. 2017.
[16] S. Sajwan, M. K. Singh, and S. Urooj, "Physical relocation of PV panel for optimization of power under PSC in PV array," in *Proc. IEEMA Engineer Infinite Conf. (eTechNxT)*, Mar. 2018, pp. 1–6.
[17] P. T. Le, H.-L. Tsai, and T. H. Lam, "A wireless visualization monitoring, evaluation system for commercial photovoltaic modules solely in MATLAB/Simulink environment," *Sol. Energy*, vol. 140, pp. 1–11, Dec. 2016.
[18] K.-H. Chao and C.-T. Chen, "A remote supervision fault diagnosis meter for photovoltaic power generation systems," *Measurement*, vol. 104, pp. 93–104, Jul. 2017.
[19] A. Triki-Lahiani, A. Bennani-Ben Abdelghani, and I. Slama-Belkhodja, "Fault detection and monitoring systems for photovoltaic installations: A review," *Renew. Sustain. Energy Rev.*, vol. 82, pp. 2680–2692, Feb. 2018.
[20] Z. Chen, L. Wu, S. Cheng, P. Lin, Y. Wu, and W. Lin, "Intelligent fault diagnosis of photovoltaic arrays based on optimized kernel extreme learning machine and I-V characteristics," *Appl. Energy*, vol. 204, pp. 912–931, Oct. 2017.
[21] Z. Chen, Y. Chen, L. Wu, S. Cheng, and P. Lin, "Deep residual network based fault detection and diagnosis of photovoltaic arrays using current-voltage curves and ambient conditions," *Energy Convers. Manage.*, vol. 198, Oct. 2019, Art. no. 111793.
[22] M. Prieto, A. Pernía, F. Nuño, J. Díaz, and P. Villegas, "Development of a wireless sensor network for individual monitoring of panels in a photovoltaic plant," *Sensors*, vol. 14, no. 2, pp. 2379–2396, Jan. 2014.
[23] F. Shariff, N. A. Rahim, and W. P. Hew, "Zigbee-based data acquisition system for online monitoring of grid-connected photovoltaic system," *Expert Syst. Appl.*, vol. 42, no. 3, pp. 1730–1742, Feb. 2015.
[24] S. Chang, Q. Wang, H. Hu, Z. Ding, and H. Guo, "An NNwC MPPT-based energy supply solution for sensor nodes in buildings and its feasibility study," *Energies*, vol. 12, no. 1, p. 101, Dec. 2018.
[25] T. Wu, M. S. Arefin, J.-M. Redoute, and M. Yuce, "A solar energy harvester with an improved MPPT circuit for wearable IoT applications," in *Proc. 11th Int. Conf. Body Area Netw.*, 2017, pp. 166–170.
[26] D. Dondi, A. Bertacchini, D. Brunelli, L. Larcher, and L. Benini, "Modeling and optimization of a solar energy harvester system for self-powered wireless sensor networks," *IEEE Trans. Ind. Electron.*, vol. 55, no. 7, pp. 2759–2766, Jul. 2008.
[27] P. Rawat, K. D. Singh, H. Chaouchi, and J. M. Bonnin, "Wireless sensor networks: A survey on recent developments and potential synergies," *J. Supercomput.*, vol. 68, no. 1, pp. 1–48, Oct. 2013.
[28] P. P. Parikh, M. G. Kanabar, and T. S. Sidhu, "Opportunities and challenges of wireless communication technologies for smart grid applications," in *Proc. IEEE PES Gen. Meeting*, Jul. 2010, pp. 1–7.
[29] V. Samavatian and A. Radan, "A high efficiency input/output magnetically coupled interleaved Buck–Boost converter with low internal oscillation for fuel-cell applications: CCM steady-state analysis," *IEEE Trans. Ind. Electron.*, vol. 62, no. 9, pp. 5560–5568, Sep. 2015.
[30] J. Lu, H. Okada, T. Itoh, T. Harada, and R. Maeda, "Toward the world smallest wireless sensor nodes with ultralow power consumption," *IEEE Sensors J.*, vol. 14, no. 6, pp. 2035–2041, Jun. 2014.
[31] C. Rubia-Marcos, J. Medina-García, J. Galán, D. Daza, and R. G. Carvajal, "Low activity mechanism for mobile sensor/actuator networks based on IEEE 802.15.4," *Wireless Pers. Commun.*, vol. 97, no. 1, pp. 197–212, May 2017.
[32] *Wireless Medium Access Control (MAC) and Physical Layer (PHY) Specifications for Low Rate Wireless Personal Area Networks (WPANs)*, IEEE Standard P802.15.4/D6, 2006.

ARANZAZU D. MARTIN was born in Bollullos del Condado, Huelva, Spain. She received the B.S. degree in industrial engineering, the M.S. and Ph.D. degrees in control engineering, electronic systems, and industrial computer science from the University of Huelva, Huelva, Spain, in 2008, 2011, and 2016, respectively. Since 2008, she has been collaborating with the Electrical Engineering Department, University of Huelva. She has been an Assistant Professor, since 2017. Her current research interests include renewable energy, distributed generation, power quality, and control systems.

J. M. CANO was born in Bollullos del Condado, Huelva, Spain. He received the degree in automatic and industrial electronic engineering and the masters' degree in automatic, robotics, and telematics from the University of Sevilla, Sevilla, Spain, in 2007 and 2008, respectively. Since 2008, he has been collaborating with the Automatic Department, University of Sevilla. Since 2019, he has been with the GIMA Research Group, University of Huelva, Spain. His current research interests include control systems, photovoltaics, unmanned aerial vehicles, and programming.

J. MEDINA-GARCÍA was born in La Palma del Condado, Huelva, Spain. He received the M.S. degree in control engineering, electronic systems, and industrial computer science, and Ph.D. degree from the University of Huelva, in 2011 and 2018, respectively. He is currently working with the Department of Electronic Engineering, Computers, and Automatic, University of Huelva, where he holds a position of researcher. His research interests include design of circuits and systems for wireless and wired communication, and embedded systems for applications in renewable energy systems.

J. A. GÓMEZ-GALÁN was born in Alosno, Huelva, Spain. He received the Electronic Engineering degree from the University of Granada, Granada, Spain, in 1999, and the Ph.D. degree (Hons.) from the School of Engineering, University of Seville, Spain, in 2003. He is currently a Full Professor with the Department of Electronic Engineering, Computers, and Automatic, University of Huelva, Spain. He was an Invited Researcher with the Klipsch School of Electrical and Computer Engineering, New Mexico State University, Las Cruces, NM, USA, in the Summer 2004. His current research interests include related to analog and mixed signal processing with emphasis on low-voltage, low-power implementations, and instrumentation systems in renewable energy systems.

JESUS R. VAZQUEZ was born in Huelva, Spain, in December 24, 1967. He received the degree in electrical engineering from the University of Seville, Spain, in 1995. For one year, he was with the Electrical Department of Nissan Motor Ibérica S. A., Barcelona, Spain. Since 1996, he has been with the Electrical Engineering Department, University of Huelva, Spain. He teaches electric circuits and power electronics. His research interests include power quality, PV systems, and neural-network applications.